UCID- 20302

PRESSURE-DENSITY BEHAVIOR FOR AlN, Al_2O_3 SiO_2, TiB_2 AND TiC POWDERS UP TO 3.5 GPa

H. C. Weed

June, 1984

Lawrence Livermore National Laboratory

This is an informal report intended primarily for internal or limited external distribution. The opinions and conclusions stated are those of the author and may or may not be those of the Laboratory.
Work performed under the auspices of the U.S. Department of Energy by the Lawrence Livermore National Laboratory under Contract W-7405-Eng-48.

Available to DOE and DOE contractors from the
Office of Scientific and Technical Information
P.O. Box 62, Oak Ridge, TN 37831
Prices available from (615) 576-8401, FTS 626-8401

Available to the public from the
National Technical Information Service
U.S. Department of Commerce
5285 Port Royal Rd.,
Springfield, VA 22161

PRESSURE-DENSITY BEHAVIOR FOR AlN, Al_2O_3, SiO_2, TiB_2 AND TiC POWDERS UP TO 3.5 GPa

H. C. Weed

June 1984

ABSTRACT

As part of a program to model the behavior of ceramic bodies suitable for high-strength, low-density applications, the pressure-density characteristics are determined for AlN, Al_2O_3, SiO_2, TiB_2, and TiC powders at 20°C and a strain rate of 2 X 10^{-4}/sec. The pressure range is 0.11 MPa to 3.5 GPa. Both the loading and unloading cycles are examined. The pressure-density behavior can be represented by an empirical equation of state similar in functional form to the Birch-Murnaghan equation. The logarithm of the net compaction decreases linearly with the initial density ratio for AlN powder, and may do so for the others. The results constitute a database for testing models of powder behavior such as the P-α model.

INTRODUCTION

The compaction of powders at high pressures to form parts for processing is a well-known technique in the fields of powder metallurgy and ceramic fabrication. Dynamic compaction with high strain rates and high maximum pressures has been used by Gourdin on powders of low-carbon-alloy steel (1983a) and Al-6% Si alloy and copper (1983b). Quasi-static compaction at low temperatures and low strain rates has been investigated by Gutmanas et al. (1979) for both brittle and ductile materials. This report presents a study of pressure-volume behavior of AlN, Al_2O_3, TiB_2, TiC, and SiO_2 powders at ambient temperature and low strain-rate. This is part of an investigation into the compaction of refractory powders at both high and low strain-rates with the long-term goal of producing ceramic bodies suitable for high-strength, low-density applications. The strain-rate is 2×10^{-4}/sec, the temperature $20^{o}C$, and the pressure range 0.11 MPa - 3.5 GPa. Results are presented for the behavior on loading-unloading paths, and for permanent compaction as a function of initial powder density.

EXPERIMENTAL PROCEDURE

Starting materials are (-325 mesh) powders with the characteristics shown in Table 1. They are stored in glass bottles sealed with screw caps but are given no special treatment before use. The AlN, TiB_2, and TiC powders have been characterized in considerable detail with respect to surface composition, size distribution, and shape (Meisenheimer, 1984). Particles of these powders all have thin surface oxide films, and are all irregular in shape. AlN is the most heterogeneous of the three; AlN composition depends on particle size but the other compositions do not.

The experimental apparatus consists of a double-acting Kennedy press controlled by an LSI-11 computer and TEK-4051 terminal. Stephens et al (1970) and Stephens and Lilley (1970) described the basic experimental arrangement. Grens (1970) described the servomechanisms and digital-to-analog converters which control the press. Figure 1 shows a view of the steel die (A) with tungsten carbide insert (B), upper anvil (D), and lower piston (C), which compresses the sample. The powder sample and reference sample assemblies are in front of the die. The reference assembly consists of a high purity solid nickel cylinder (G) contained in a tin jacket and lid (E) (Fig. 1, lower right). The ends are sealed by ring-and-wafer units (F) to prevent extrusion of tin past the piston (C) and anvil (D) during a run. The powder sample assembly is identical to the reference sample assembly except that it contains powder (H) loaded to the appropriate initial density.

As the first step in the experimental procedure, the powder sample is prepared in the die in which it will be run. The tin jacket is loaded into the die on top of a ring-and-wafer assembly and the tungsten carbide anvil (D). Three equal amounts of powder (with weight determined by the desired initial density) are pressed into the tin jacket using an auxiliary press and a series of spacers between the die and the face of the press ram to control the volume occupied by the powder at each stage of pressing. When the powder has been compressed to the requisite initial density, the tin lid is inserted. The ring-and-wafer seal is added next, and finally the tungsten carbide piston (C). The loaded die assembly is then placed in the Kennedy press with the anvil at the top, since the piston is driven into the die by the lower ram of the Kennedy press. End loading is applied to the die assembly by the upper ram in order to avoid fracture of the carbide die at high pressures.

The sample is cycled in pressure; the initial conditioning cycle is from 0.11 - 50 MPa, and subsequent data collection cycles are from 0.11 MPa to 3.5 GPa. Load and piston displacement are recorded at intervals preset by the LSI-11 computer which drives the press. In order to standardize the performance of the die and press, a solid nickel reference sample is processed after each powder sample in the same way using the same die. A new nickel sample is used for each new powder sample.

RESULTS AND DISCUSSION

At the end of each complete experiment there are two sets of load vs piston displacement data, one set for the powder sample and the other for the Ni reference sample. The load values are corrected for frictional effects and converted to pressures, which are stored in pressure vs. displacement arrays. The pressure values in these arrays are the same because the powder and Ni runs were conducted over the same range of pressures and sampled at the same pressure intervals. Therefore, corresponding to each pressure value there are displacement values for powder and for Ni. From these the differential displacement and differential sample volume can be calculated as a functon of pressure. Finally, the powder volume is calculated from the differential volume and the volume of Ni given by the Ni equation of state.

The pressure-volume data were analyzed by the method of least-squares using the following equations:

$$u = L_0 + L_1 y + L_2 y^2 \tag{1}$$

where u is calculated from

$$u = P/((y + 1)^{5/2} y) \tag{2}$$

and

$$y = ((\rho/\rho_0)^{2/3} - 1) = ((V/V_0)^{-2/3} - 1). \tag{3}$$

V, ρ are the specific volume and density of the powder sample at pressure P, and V_0, ρ_0 the specific volume and density at P = 0.11 MPa $\simeq$ 0 before the start of the run. L_0, L_1, L_2 are empirically determined constants from the least-squares analysis. Equations (1) - (3) are similar in functional form to the Birch-Murnaghan equation for elastic solids (Weaver et al., 1971), but cannot be interpreted in detail in terms of elastic solid theory when used for the powders. This functional form has been shown to be suitable for data with a large maximum strain (about 25%) and non-linear variation. The loading curve and unloading curve are analyzed separately. After analysis, values of the pressure (P) are calculated as a function of (ρ/ρ_{so}) from

$$P_c = ((y + 1)^{5/2} y) u_c \tag{4}$$

and

$$(\rho/\rho_{so}) = (\rho/\rho_0)/(\rho_{s0}/\rho_0). \tag{5}$$

where u_c is the calculated value of u from the least squares analysis and ρ_{s0} is the density of the solid at 100% theoretical density and 0.11 MPa pressure. Standard deviations in the pressures are estimated from:

$$\sigma^2 = \sum_i (P_i - P_{ci})^2 / (n-k) \tag{6}$$

Here, σ is the standard deviation, P_i is the i-th measured pressure, P_{ci} is the ith calculated pressure from (4) and (5) above, i is the index from 1 to n, n is the number of data, and k is the number of parameters whose values are determined during least-squares analysis. For the present case, k=3. Values of the standard deviation are shown in Table 2. All are less than 0.1 GPa except for Al_2O_3 sample No. 2, for which σ = 0.12 GPa. A reference curve was calculated for each powder from the Birch-Murnaghan equation of state of the corresponding solid. It is assumed that the solid is at 100% theoretical density and that K the bulk modulus is either constant, or shows a linear dependence on the pressure. The equation is

$$u = A_0 + A_1 y \tag{7}$$

where u is calculated from (2) and (3) above for the least-squares analysis, and P_c vs (ρ/ρ_{s0}) is calculated from (4) and (5) after A_0 and A_1 have been determined. Input values of P and V/V_0 for the least squares analysis were obtained from the data of Bridgman (1949) on single crystal sapphire, and Bridgman (1948) on α-quartz.

For AlN and for TiC, input values of P and V/V_0 were calculated from the Mie-Gruneisen equations of Horie et al. (1983). No least squares analysis was done in the case of TiB_2. Instead, A_0 and A_1 were calculated from expressions in (Weaver et al., 1971):

$$A_0 = 3/2\ K_0 \tag{8}$$

$$A_1 = A_0\ (3/4\ K'_0 - 3). \tag{9}$$

K'_0 is assumed to be zero; K_0 is taken as the average of the Voigt and Reuss acoustic values for K from Simmons and Wang (1971). The results are shown in Figs. 2-6 as plots of P vs (ρ/ρ_{s0}) and in Table 2 as values of L_0, L_1, L_2. Values of P calculated from (4) and (5) above are shown by solid lines. Arrows show increasing time.

In Fig. 3, results on the hydrostatic compaction of TiC by Bumm and Liepelt (1972) are shown by X's. These authors do not give complete P vs. (ρ/ρ_{so}) curves, but show the maximum compacting pressure vs. the final (ρ/ρ_{so}) for each compacted sample. The results in Fig. 3 are maximum pressure and maximum (ρ/ρ_{so}); since all samples are assumed to have the same initial density, the results are interpreted as loading curves. Values of maximum (ρ/ρ_{so}) are calculated from Bumm and Liepelt's data on the assumption that their unloading curves have the same slope in P - (ρ/ρ_{so}) space as those of the present investigation. The initial density of their samples is similar to that of Sample 2; their samples are more compressible below 1 GPa, but about equally compressible above 1 GPa. The results of Horie et al for AlN are shown as X's in Fig. 4. They were calculated from the Horie et al isostatic compaction data in the same way as shown above for TiC. They are to be compared with the results for Sample 5 (+). The agreement between the two data sets for AlN is close.

The unloading curves have fewer data than the loading curves because frictional corrections on unloading are large and uncertain at the highest pressures; therefore, the highest-pressure unloading data are omitted. The number of omitted data is 12 to 15. As shown in the graph for each composition, the unloading curves are steeper than the loading curves. The powders, which have already been compacted at 3.5 GPa, behave more like completely dense solids than they did at the start of the runs. One unloading curve for SiO_2 appears anomalous in that it crosses the loading curve (Sample No. 2, Fig. 9). This was caused by breakage of the piston during the latter part of the loading cycle.

AlN sample No. 9 is interesting since it was prepared by machining a sintered bar which had about 30% porosity. It behaves similarly to powder samples of AlN having the same initial density, which suggests that powders and porous solids might be modeled in the same way.

Agreement between observed and calculated values of P is usually better above 0.2 GPa for the unloading cycles than the loading cycles, for the following reasons: (1) The function u is very sensitive to fluctuations in (V/V_0) or (ρ/ρ_0) when (ρ/ρ_0) is close to 1, which occurs for the powders from about 0.2 GPa to 0.01 GPa. (2) Inspection of the least-squares analysis plots of u vs. y shows that the low-pressure behavior is more erratic for the loading cycles than the unloading cycles. A possible explanation is that the particles in the uncompacted powders can translate, rotate, or form temporary bridges more easily than in the compacted ones. (3) The results are heavily weighted toward low-pressure behavior since there are 20 data from .01 to .19 GPa, out of a total of 56 to 60 for a loading run, and 32 to 36 for an unloading run.

In order to correlate the behavior of the powders with that of the solids the change in density ratio with pressure is separated into the increase for the loading cycle and the decrease for the unloading cycle. Table 3 gives results taken from the P vs. (ρ/ρ_{so}) curves of Figs. 2-6, together with literature values of the shear modulus (G) and the modulus of elasticity (E) for the solids. Figure 7 shows Δ_1 the increase during the loading cycle as a function of the initial density ratio. Δ_1 is defined as:

$$\Delta_1 = (\rho/\rho_{so})_{max.} - (\rho/\rho_{so})_{initial} \qquad (10)$$

The results appear to lie on a family of straight lines, of approximately equal slope. SiO_2 is separate from the other four compositions, which lie in a group nearer to the origin of coordinates. The positions of the lines are correlated with the values of G and E: SiO_2 has low values of G and E, whereas the other compositions have high values of G and E. The decrease for the unloading cycle is shown as - Δ_2 vs. the initial density ratio (Fig. 8) whre Δ_2 is defined as

$$\Delta_2 = (\rho/\rho_{so})_{final} - (\rho/\rho_{so})_{max.} \tag{11}$$

The results again fall into two groups: SiO_2 with Δ_2 between -.14 and -.17, and the rest of the compositions with Δ_2 between -.02 and -.08.

SiO_2 has a much lower G and E than the other compositions (Table 3) and a much larger increase in density ratio during loading (Fig. 7). SiO_2 may have welded to some extent during loading, which accounts for the permanent increase in density ratio, but most of its response was probably elastic. Al_2O_3 remains hard and brittle under triaxial loading up to a confining pressure of 1.25 GPa (Heard and Cline, 1980); on the basis of the work of Bridgman (1952), Heard and Cline also surmise that elastic behavior continues up to 3.5 GPa. During the loading cycle, Al_2O_3 grains were not welded, but broken up and rearranged, with the amount of breakage increasing with the initial density ratio. AlN shows ductile behavior above 0.55 GPa confining pressure under triaxial loading (Heard and Cline, 1980). Also, the small particle size (50μm diameter) may have contributed to welding during the loading cycle, producing permanent compaction. TiB_2 and TiC have such high shear and elastic moduli that they probably deformed by particle rearrangement during loading, and were able to achieve close, stable packing because of the small particle size (9μm and 3μm respectively).

In order to increase the usefulness of this study for describing compaction behavior of the powders, the net compaction and calculated final density ratio values are shown as a function of the initial density ratio. The net compaction Δ is:

$$\Delta = (\rho/\rho_{so})_{final} - (\rho/\rho_{so})_{initial} \tag{12}$$

As shown in Fig. 10, log Δ is a linear function of the initial density ratio in the case of AlN:

$$\log \Delta = D_0 + D_1 \, (\rho/\rho_{so})_{initial} \tag{13}$$

Least-squares analysis gives $D_0 = 0.6320 \pm .055$ and $D_1 = -2.156 \pm .080$. The standard deviation (σ) in log Δ is 0.0093 which corresponds to a 2% deviation in Δ for AlN. The slopes appear similar for all compositions except Al_2O_3. The data for AlN, TiB_2, and SiO_2 are so close together that the differences among them may not be significant. TiC has a lower intercept than the other three, and Al_2O_3 the lowest of all. Horie et al. (1983) have reported results from compaction experiments on AlN at various maximum pressures. Their result at 3.4 GPa maximum pressure is shown in Fig. 9(H). There is good agreement between it and the results of this study, at an initial density ratio of 0.6. Equations (12) and (13) can be solved for the final density ratio:

$$(\rho/\rho_{so})_{final} = (\rho/\rho_{so})_{initial} + 10^{(D_0 + D_1 (\rho/\rho_{so})_{in.})} \tag{14}$$

The calculated value of the final density ratio has a minimum with respect to the initial density ratio, as shown in Figure 10 for AlN. The result from the isostatic compaction experiments of Horie et al. (1983)(H) is somewhat higher than those from the present study, at an initial density ratio of 0.6.

Quasi-hydrostatic compaction of powders at low strain-rates is described by the data in this study, and Equations (1) to (5). In order to apply the results to conditions characteristic of shock wave experiments, theoretical models must be tested, using the experimental results as a database. It appears that the P-α model applied to porous solids by Bhatt et al. (1975) and Carroll (1980), and to AlN and TiC powders by Horie et al. (1983) would be a good choice. This model requires a substantial calculational effort which is beyond the scope of the present study. Therefore, the application of the model should be considered as a separate program.

At this time, characterization of the pre- and post-run samples from the quasi-hydrostatic experiments is the next thing that should be done. This includes X-ray analysis and TEM examination to determine the extent (if any) of permanent deformation of the crystal structure of the powder particles, and microscopic examination to determine particle morphology. The Al_2O_3 and SiO_2 starting materials should also be characterized as the AlN, TiB_2, and TiC have been. The result will be a useful database on which the P-α model or other possible models can be tested, and which can be expanded wherever necessary.

CONCLUSIONS

The most important conclusions from this investigation are as follows:

- The quasi-hydrostatic pressure-density behavior of AlN, Al_2O_3, SiO_2 TiB_2 and TiC powders can be represented by an empirical equation of state similar to the Birch-Murnaghan equation.

- The log of the net compaction of AlN decreases linearly with the initial density ratio, and may do so for the other powders studied.

- An expression is given to calculate the final density ratio for AlN from the initial density ratio, under a maximum pressure of 3.4 GPa.

- An attempt should be made to test the P- α model against the quasi-hydrostatic data from this investigation. Because of the large calculational effort required, the attempt should be set up as a separate study.

ACKNOWLEDGMENT

I wish to thank the following people for the people for their help. Hugh Heard suggested the problem and provided constructive criticism and encouragement. Carl Cline provided advice and program support. Stan Lanning wrote and maintained the data acquisition and reduction programs, KEN3 and ROCK. Eben Lilley was always available for advice on experimental technique and Carl Boro provided essential mechanical support. The report was reviewed by G. Anderson, J. Berryman, B. Bonner, A. Duba, A. Kusubov, and W. Lin.

REFERENCES

Bernstein, H. (1964), Met. Soc. AIME, Inst. Metals Div. Spec. Rept. Series, No. 13, 193-213.

Bhatt, J. J., M. M. Carroll and J. F. Schatz (1975), A Spherical Model Calculation for Volumetric Response of Porous Rocks, J. Appl. Mech., 42, 363-368.

Bridgman, P. W. (1948), The compression of 39 substances to 100,000 kg/cm^2, Proc. Am. Acad. Arts Sci., 76, 55-70, in Collected Experimental Papers, Vol. VI, Harvard Univ. Press (1964) 160:68.

Bridgman, P. W. (1949), Linear compressions to 30,000 kg/cm^2 including relatively incompressible substances, Proc. Am. Acad. Arts Sci., 77, 189-234, in Collected Experimental Papers, Vol. VI, Harvard Univ. Press (1964) 168:222.

Bridgman, P. W. (1952), Studies in Large Plastic Flow and Fracture, McGraw Hill, New York.

Bumm, H. and H. Liepelt (1972), Versuchsergebnisse mit einer isostatischan Preßanlage für Drücke bis 15000 Atmosphären an metallischen and nichtmetallischen Pulvern, Zts. für Werkstofftechnik, 3, 364.

Burnett, S. J. (1964), Properties of Refractory Materials, AERE-R4657, Engineering Division, AERE, Harwell, Berks., U.K. (1964).

Carroll, M. M. (1980), Compaction of Dry or Fluid-Filled Porous Materials, J. Engrg. Mech. Div., ASCE, 106 EM5, 969-990.

DeKlerk, J. (1965), Elastic constants and Debye temperature of TiC using a new ultrasonic coherent pulse/cw technique, Rev. Sci. Inst. 36, 1540-1545.

Gilman, J. J. and B. W. Roberts (1961), Elastic Constants of TiC and TiB_2, J. Appl. Phys. 32, 1405, in Gene Simmons and Herbert Wang, Single Crystal Elastic Constants and Calculated Aggregate Properties: A Handbook, 2d ed., The M.I.T. Press, Cambridge, MA and London, England (1971).

Gourdin, W. H. (1983a), Energy Deposition and Microstructural Modification in Dynamically Consolidated Powders.II.Application to 4330V Powder. UCRL 88902, Part 2, Preprint. Lawrence Livermore National Laboratory, May (1983).

Gourdin, W. H. (1983b), Energy Deposition and Microstructural Modification in Dynamically Consolidated Powders.III.Application to Al-6%Si Alloy and Copper. UCRL 88902, Part 3, Preprint. Lawrence Livermore National Laboratory, May (1983).

Grens, John Z. (1970), Computer operation of a compressibility testing apparatus, UCIR-457, Lawrence Livermore National Laboratory, April 15, 1970.

Gutmanas, E. Y., Y. Rabinkin, and M. Roitberg (1979), Cold sintering under high pressure, Scripta Metallurgica, 13, 11-15.

Heard, H. C. and C. F. Cline, (1980) Mechanical behavior of polycrystalline BeO, Al_2O_3 and AlN at high pressures, J. Materials Sci., 15, 1889-1897.

Horie, Y., J. B. Park, D. E. P. Hoy and J. K. Whitfield (1983), High Pressure Equation of State for Metal and Ceramic Powders, Final Report, Part I, Vol. 2, Support of DARPA Program in Dynamic Synthesis of Materials, North Caroline State Univ., Raleigh, NC, December (1983).

Komeya, K. and F. Noda (1974), Aluminum nitride and silicon nitride for high temperature vehicular gas turbine engines, Toshiba Review, No. 92, 13-18 (July/Aug. 1974), in Engineering Property Data on Selected Ceramics, Volume I, Nitrides. Metals and Ceramics Information Center, Battelle, Columbus Laboratories, Columbus OH 43201 (March 1976) p. 5.3.2.1-4.

McSkimin, H. J., P. Andreatch, Jr. and R. N. Thurston (1965), Elastic moduli of quartz versus hydrostatic pressure at 25° and -195.8°C, J. Appl. Phys., 36 1624-1632.

Meisenheimer, R. G. (1984), Personal communication, Lawrence Livermore National Laboratory (April 1984). DARPA Materials Synthesis Program. Materials Acquisition and Characterization.

Simmons, Gene and Herbert Wang (1971), Single Crystal Elastic Constants and Calculated Aggregate Properties: A Handbook, 2d ed., The M.I.T. Press, Cambridge, MA, and London England (1971), p. 287.

Stephens, D. R. and E. M. Lilley (1970), Loading-Unloading Pressure-Volume Curves for Rocks, in Symposium on Engineering with Nuclear Explosives, January 14-16 (1970), Las Vegas, Nevada. Proceedings. CONF-70010 (Vol. 1) USAEC May (1970), pp. 89-109.

Stephens, D. R., E. M. Lilley and H. Louis (1970), Pressure-Volume Equation of State of Consolidated and Fractured Rocks to 40 kb, Int. J. Rock Mech. Min. Sci., 1, 257-96.

Storms, Edmund K. (1967), The Refractory Carbides, Academic Press, New York and London, pp. 6-8.

Taylor, K. M., and C. Lenie (1960), Some properties of aluminum nitride, J. Electrochem. Soc., 107, 308-14, in Engineering Property Data on Selected Ceramics, Volume I. Nitrides. Metals and Ceramics Information Center, Battelle, Columbus Laboratories, Columbus, OH (1976), p. 5.3.2.1-4.

Wachtman, J. B., Jr., W. E. Trefft, D. G. Lam, Jr. and R. P. Stinchfield (1960) Elastic constants of single crystal synthetic corundum at room temperature, J. Res. Nat. Bur. Stand. 64A 213-228.

Weaver, J. Scott, Taro Takahashi, and William A. Bassett, Calculation of the P-V Relation for Sodium Chloride up to 300 kilobars at 25^{o}C, in Accurate Characterization of the High Pressure Environment, Edward C. Lloyd, ed., NBS Special Publication 326, NBS, Washington D.C., March (1971), pp. 189-199.

Table 1. Characteristics of Refractory Powders

Formula	Supplier*	B.E.T. Surface Area, (a)** (b), m^2/g	Diameter, $\mu m^{(a)}$ From Surface Area	From Sedimentation(c)	Density, Mg/m^3 Solid	X-Ray, Calc.
AlN	2	2.40	0.9	50	3.19(g)	3.26(g)
TiB_2	2	0.67	2.0	9	4.50(h)	4.497(f)
TiC	2	2.19	0.55	3	4.51-4.91(c)	4.908(e)
SiO_2	3	--	--	--	2.648(h)	2.648(d)
Al_2O_3	1	--	--	--	3.97(h)	3.987(d)

*1 Reynolds Metal Co., Bauxite, Ark. 72011. High Purity Alumina RC-HP-DBM, without MgO.

2 Hermann Starck, Berlin.

3 Alfa Products, P. O. Box 299, 152 Andover St., Danvers, MA 01923

**(a) Meisenheimer (1984)

(b) Calculated assuming all particles to be equal-sized spheres

(c) 50% values from cumulative distribution curves of equivalent spherical diameter

(d) Handbook of Chemistry and Physics, 55th ed., CRC Press, Robert C. Weast, ed., p. 13-208.

(e) Storms (1967)

(f) Bernstein (1964)

(g) Taylor and Lenie (1960)

(h) Burnett (1964)

Table 2. Values of L_0, L_1, L_2 from Equations (1) and (7) and Standard Deviation Between Observed and Calculated Pressures

Sample		Initial (ρ/ρ_{so})	Loading* L_0		Loading* L_1		Loading* L_2		Unloading* L_0		Unloading* L_1		Unloading* L_2		Standard Deviation Load	Standard Deviation Un-load	Symbol
AlN	5	.593	1.36	.04	-4.5	.8	77	2	243	14	-1939	103	3865	193	.028	.054	+
	6	.673	8.29	.18	-2.1	5.8	187	31	392	27	-5226	340	17421	1064	.024	.089	♦
	7	.710	9.51	.34	53	14	-133	89	86	7	-1514	107	6646	394	.067	.049	0
	8	.748	23.4	.9	-112	47	610	392	68	14	-1700	257	10341	1204	.051	.054	*
	9	.698	14.9	.7	-56	26	243	159	81	4	-1343	67	5559	236	.079	.039	•
Solid		1	298.4	.4	-455	7	0	--	--	--	--	--	--	--	--	--	
Al_2O_3																	
	1	.612	61.9	.07	34	2	-22	13	22	1	-422	21	2060	78	.031	.034	0
	2	.681	11.7	.7	289	34	-1913	303	-6.7	1.8	-4	48	2152	302	.120	.030	+
Solid		1	413	2	-1436	455	0	--	--	--	--	--	--	--	--	--	
SiO_2	2	.663	.91	.03	-3.2	.3	48.8	.9	8.1	.4	-96	4	288	9	.024	.020	0
	3	.818	7.6	.3	31	11	149	71	-4.5	.4	96	11	291	62	.050	.026	+
Solid		1	49.6	.9	285	12	0	--	--	--	--	--	--	--	--	--	
TiB_2	2	.625	2.6	.04	-12.1	.9	160	3	109	9	-1203	90	3316	222	.030	.055	0
	3	.718	8.8	.4	76	19	-162	139	51	9	-1191	159	6881	700	.067	.054	+
Solid #		1	625.9		-1878		0	--	--	--	--	--	--	--	--	--	
TiC	1	.654	1.1	.05	-1.0	.8	69	3	76	6	-694	46	1594	93	.041	.050	0
	2	.787	18.6	.8	-136	35	868	26	18	7	-569	124	3924	544	.031	.053	+
Solid		1	319	1	2801	29	0	--	--	--	--	--	--	--	--	--	

*Results are shown as mean value ± standard deviation
#Not obtained by least squares analysis

Table 3. Density Ratios, Maximum Pressure(P_{max}), Shear Modulus (G) and Elastic Modulus (E) for SiO_2, AlN, Al_2O_3, TiB_2, and TiC

Sample	No.	Initial	ρ/ρ_{os} Max*	Final	P_{max}, GPa*	Δ_1	$-\Delta_2$	Δ	G GPa (solid)	E GPa (solid)
SiO_2	2	.664	.996	.826	3.40	.332	.170	.162	44(b)** (c)	96(b) (c)
	3	.817	1.007	.868	3.50	.190	.139	.051		
AlN	5	.593	.862	.822	3.60	.269	.040	.229	136(a)	340(a)
	6	.673	.876	.822	3.50	.203	.054	.149		
	7	.710	.881	.822	3.50	.171	.045	.126		
	8	.748	.894	.854	3.40	.146	.040	.106		
	9	.699	.884	.827	3.40	.185	.057	.128		
Al_2O_3	1	.613	.790	.710	3.40	.177	.080	.097	163 (b)	403 (b)
	2	.681	.840	.787	3.40	.123	.017	.106	(d)	(d)
TiB_2	2	.626	.854	.802	3.50	.228	.052	.176	169 (b)	446 (b)
	3	.717	.871	.823	3.40	.154	.048	.106	(e)	(e)
TiC	1	.566	.814	.757	3.50	.248	.057	.191	190 (b)	408 (b)
	2	.680	.830	.779	3.40	.150	.051	.099	(f)	(f)

*$(\rho/\rho_{os})_{max}$ corresponds to P_{max}

**(a) From E = 340 GPa and Poisson's ratio = 0.25; Taylor and Lenie (1960), Komeya and Noda (1974)

(b) Average of Voigt and Reuss values or Voigt, Reuss, Hashin and Shtrikman values (Simmons and Wang [1971]).

(c) McSkimin et al (1965) in (Simmons and Wang, 1971).

(d) Wachtman et al (1962) in (Simmons and Wang, 1971).

(e) Gilman and Roberts (1961) in (Simmons and Wang, 1971)

(f) DeKlerk (1965) in (Simmons and Wang, 1971).

Fig. 1. Die assembly, powder sample, and nickel reference sample. A - steel die. B - tungsten carbide insert. C - tungsten carbide piston. D - tungsten carbide anvil. E - tin jacket and lid. F - wafer and sealing ring. G - nickel reference sample. H - powder sample.

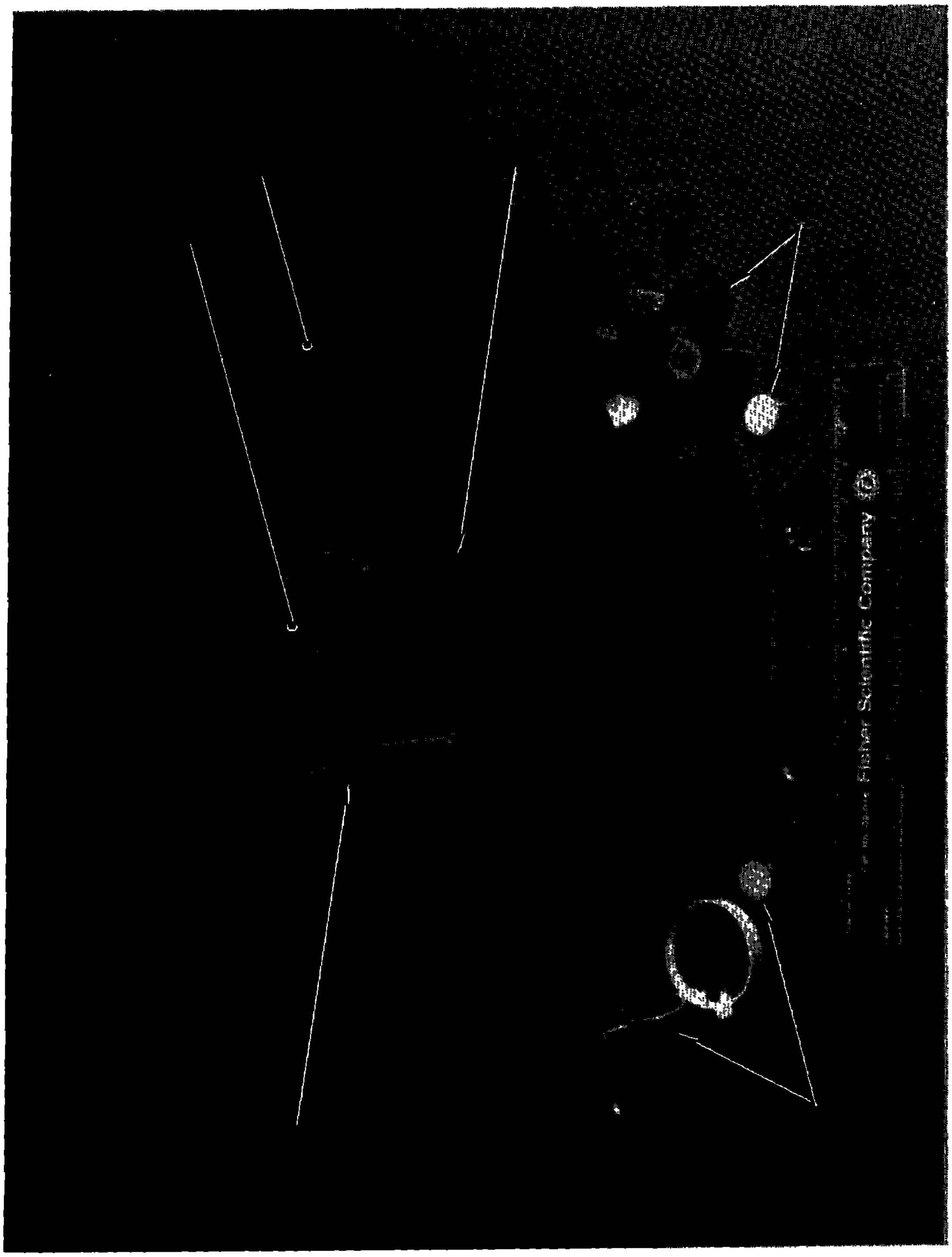
Fisher Scientific Company

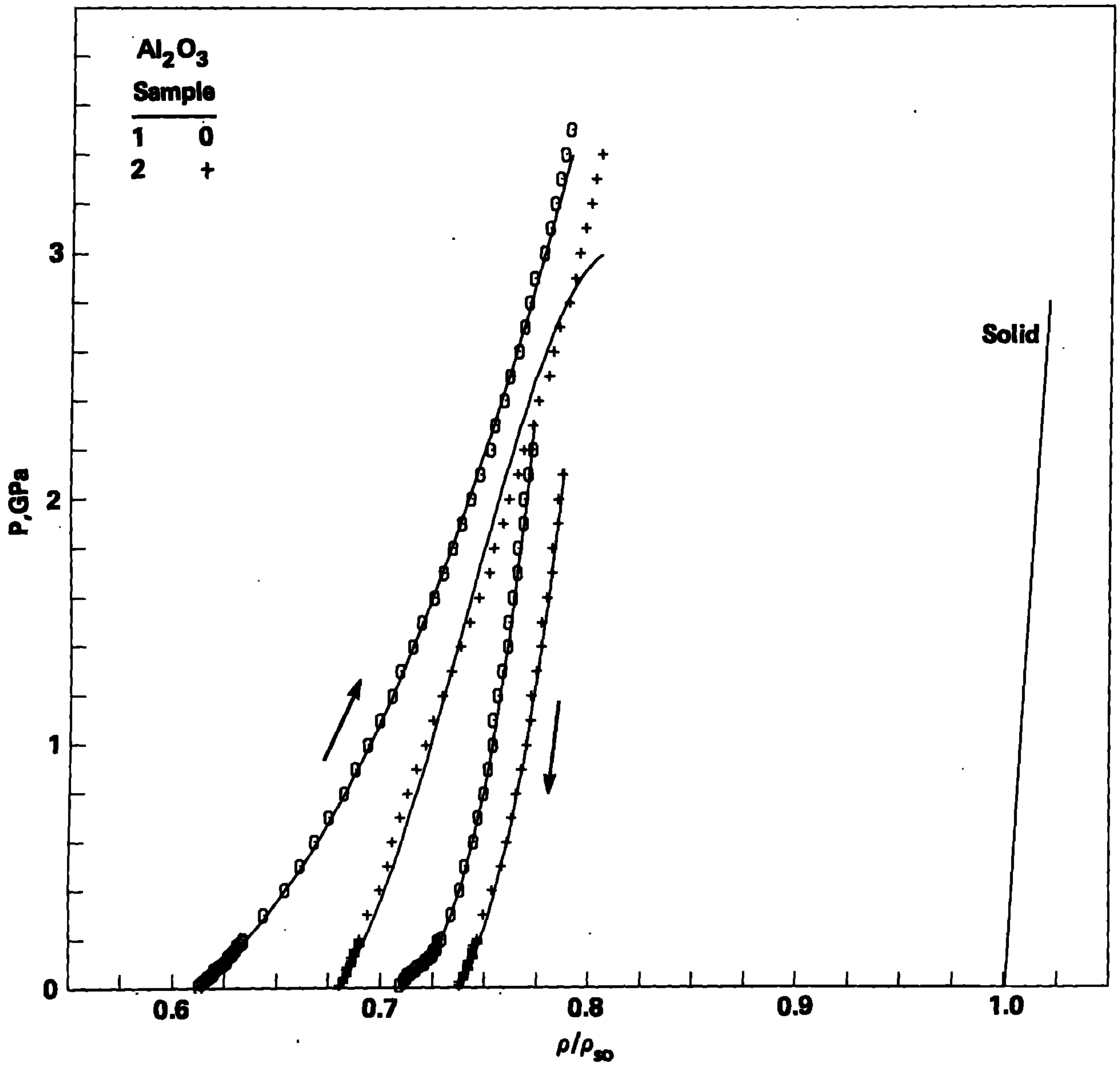

Fig. 2. P vs. (ρ/ρ_{so}), Al_2O_3. Sample No. 1 O. Sample No. 2 +.

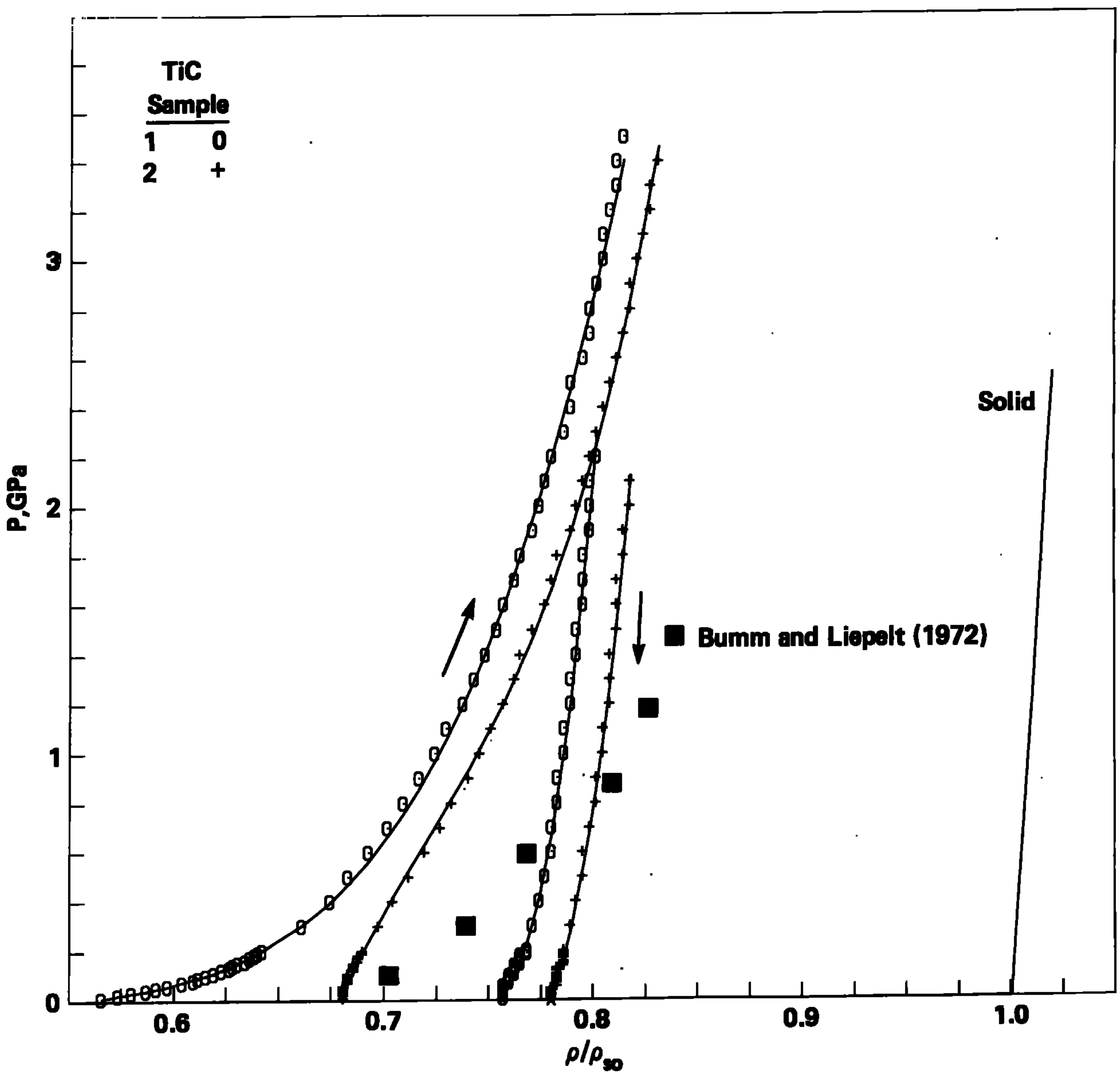

Fig. 3. P vs. (ρ/ρ_{SO}), TiC. Sample No. 1 O. Sample No. 2 +. Results of Bumm and Liepelt (1972) ■

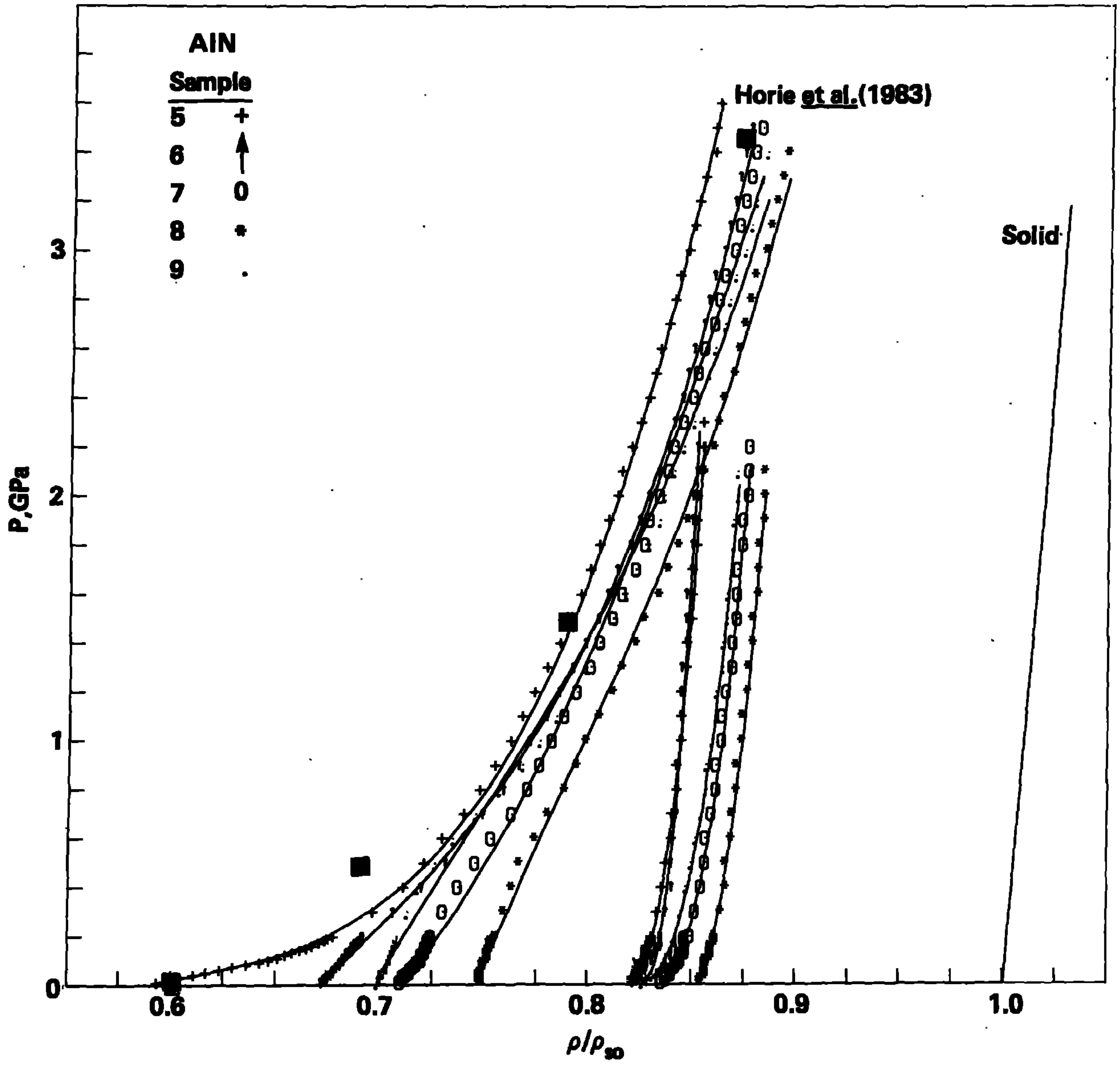

Fig. 4. P vs. (ρ/ρ_{so}), AlN. Sample No. 5 +. Sample No. 6 . Sample No. 7 0. Sample No. 8 *. Sample No. 9 •. Solid lines are calculated from least-squares analysis. Results of Horie _et al_ (1983) ■

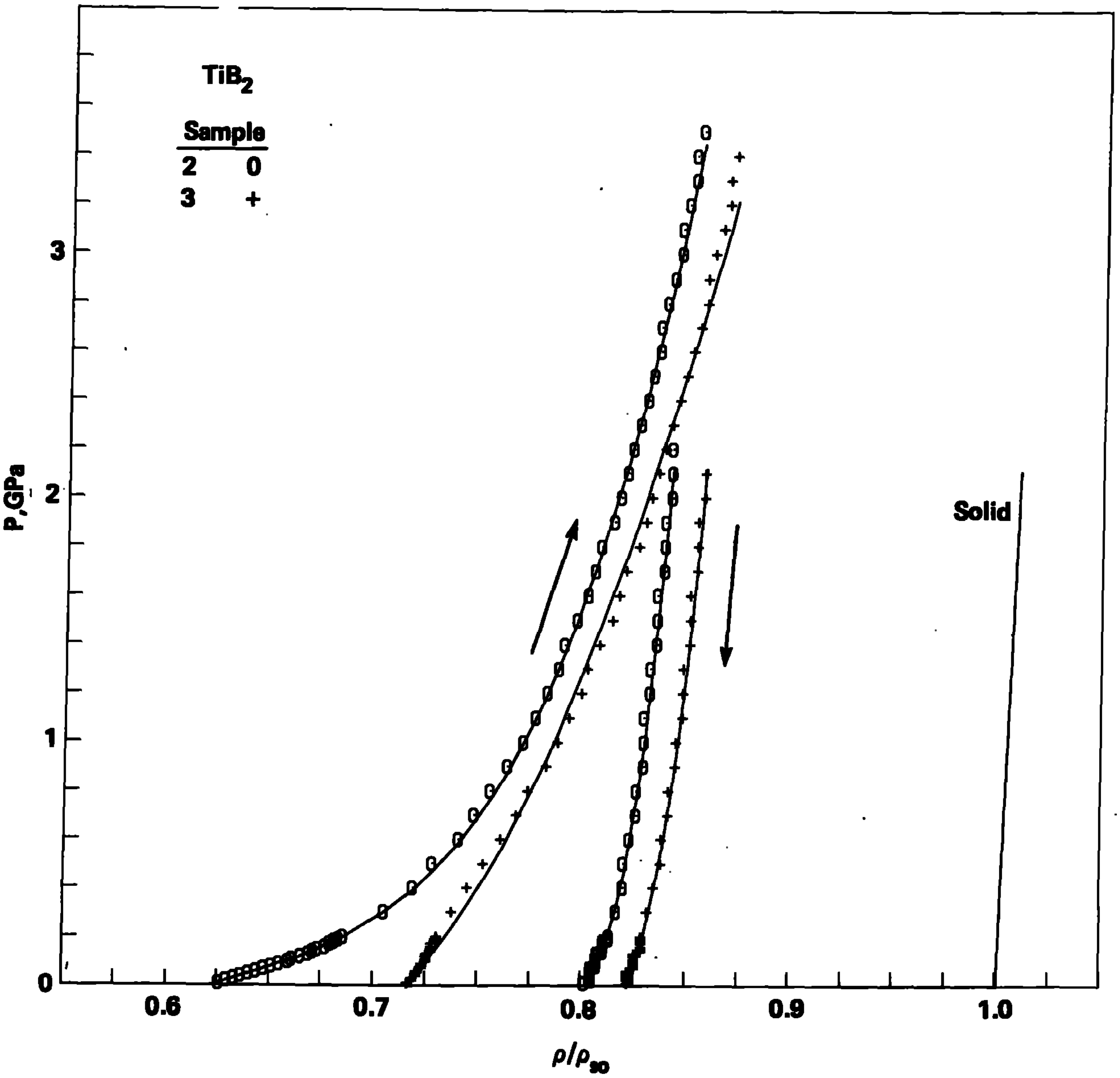

Fig. 5. P vs. (ρ/ρ_{SO}), TiB_2. Sample No. 2 O. Sample No. 3 +.

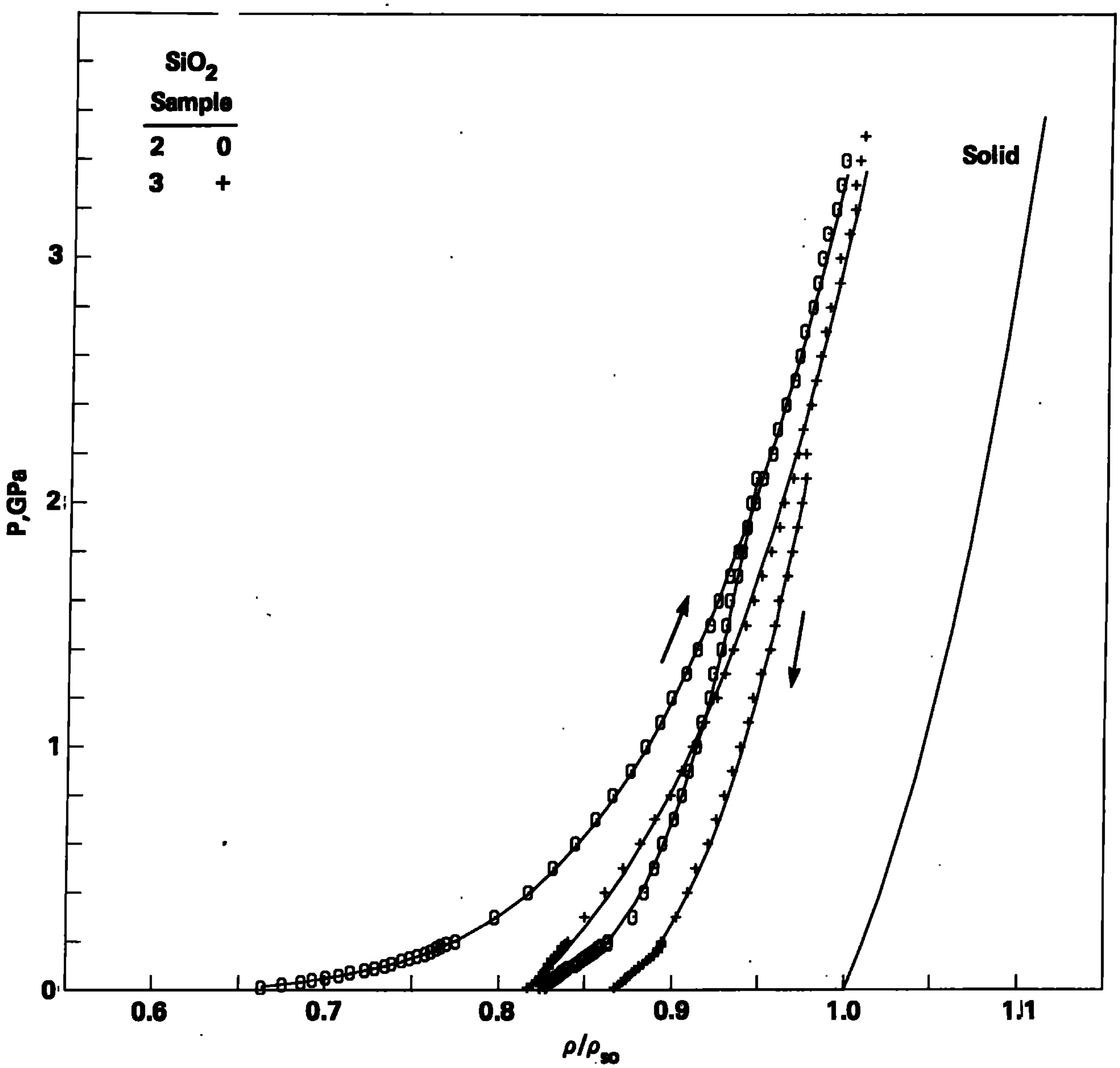

Fig. 6. P vs. (ρ/ρ_{so}), SiO_2. Sample No. 2 O. Sample No. 3 +.

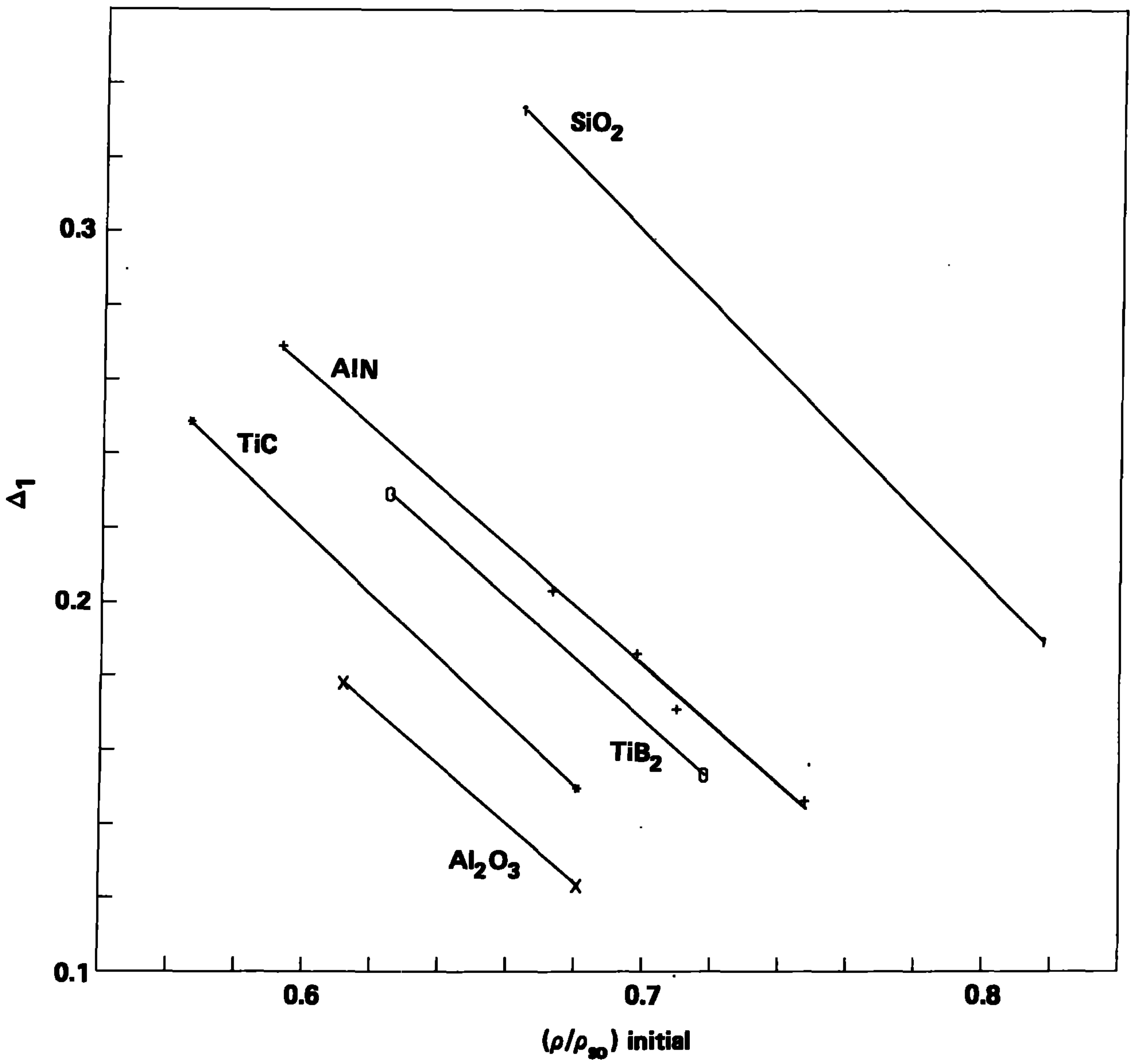

Fig. 7. Δ_1, vs. $(\rho/\rho_{so})_{initial}$, all compositions.

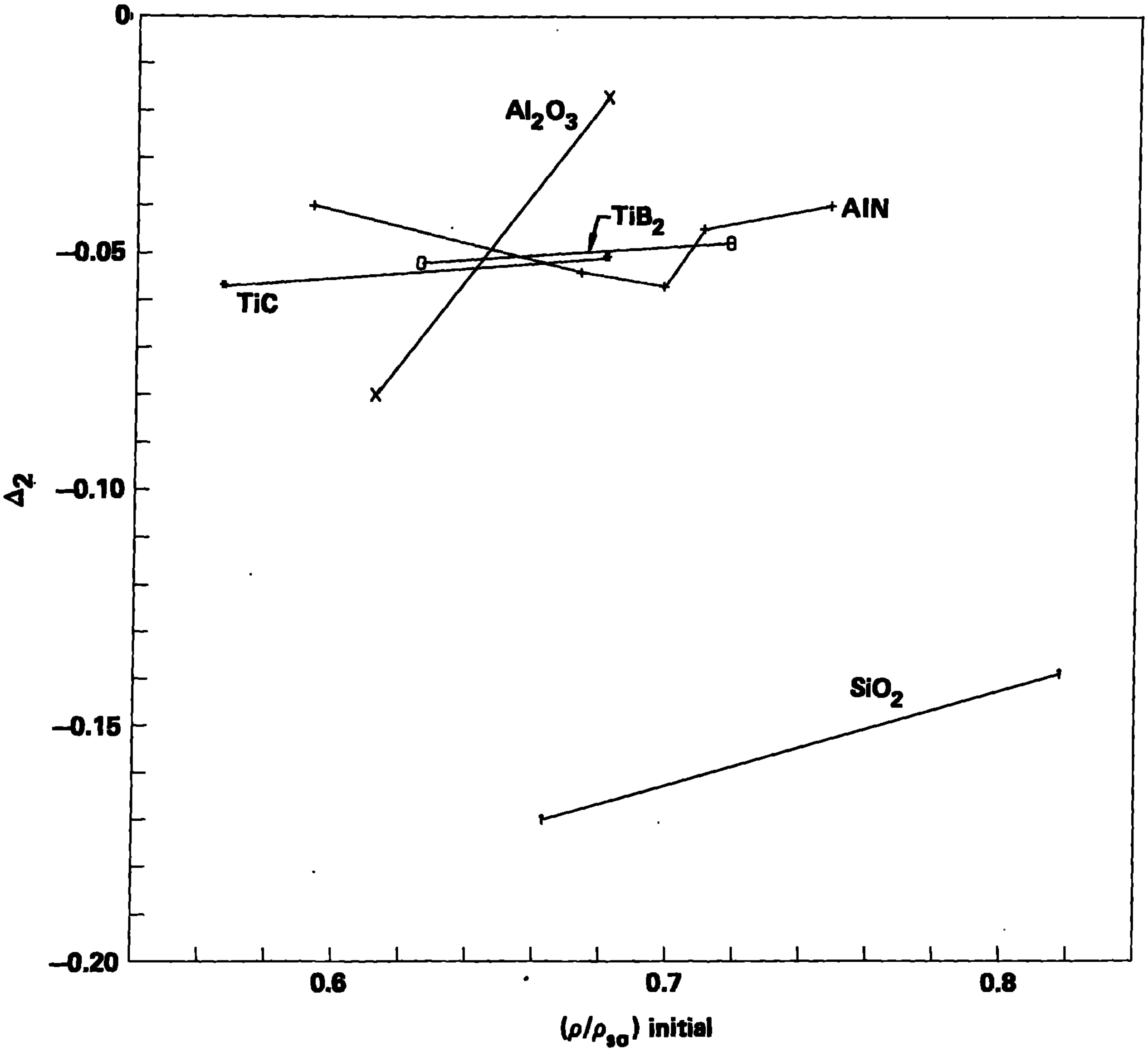

Fig. 8. Δ_2, vs. $(\rho/\rho_{so})_{initial}$, all compositions.

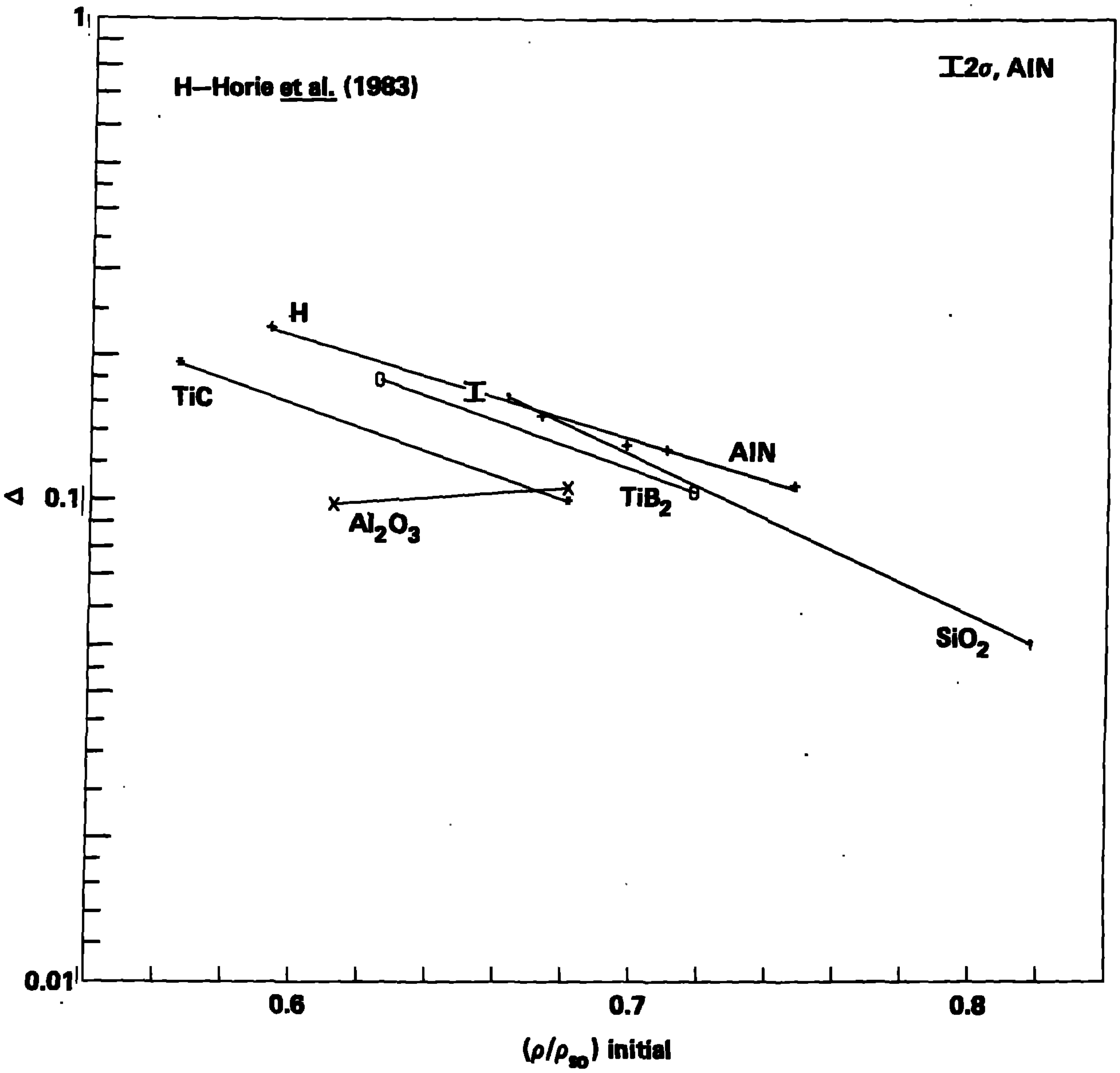

Fig. 9. Δ, vs. $(\rho/\rho_{so})_{initial}$, all compositions. H - result from Horie et al. (1983).

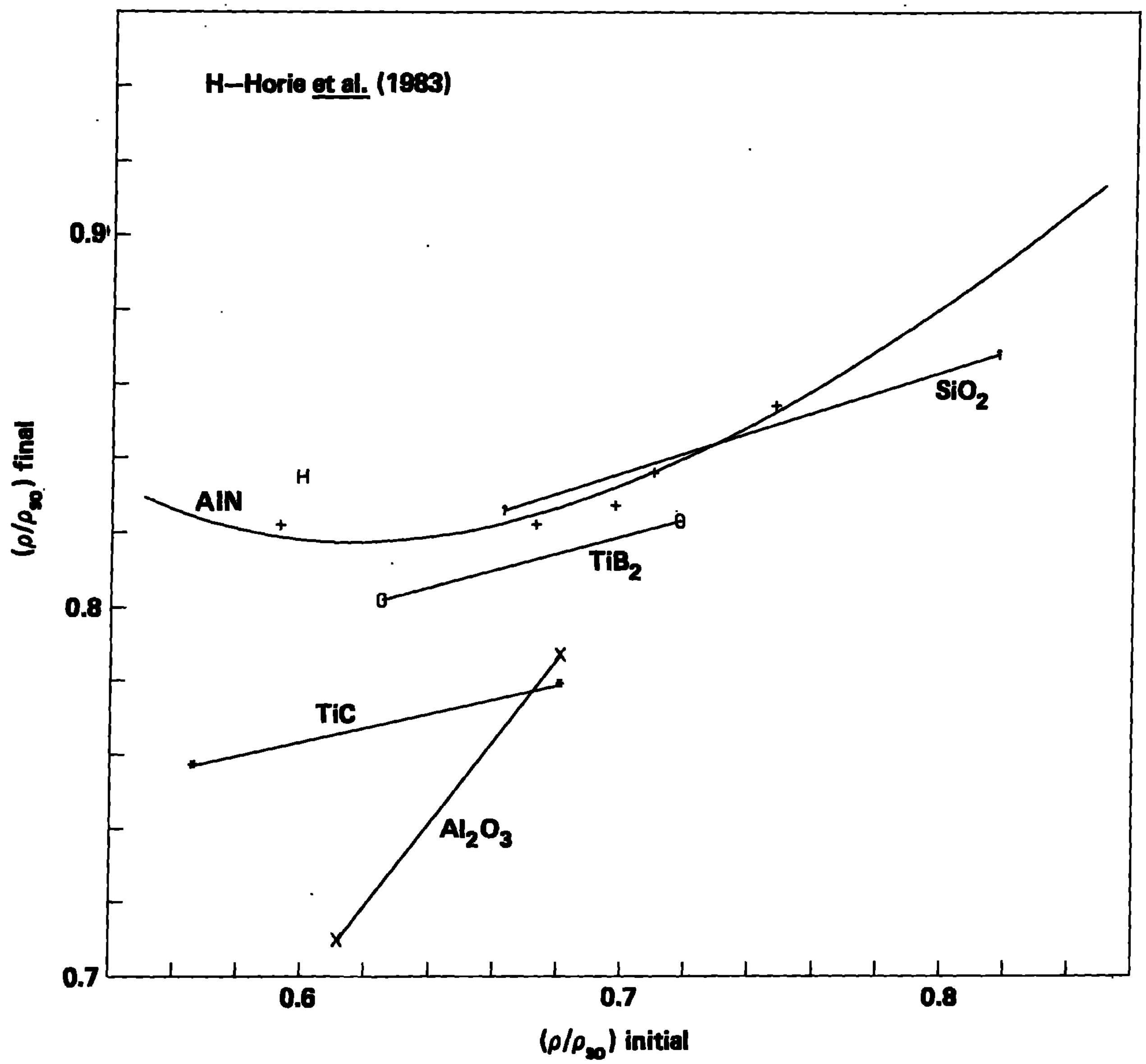

Fig. 10. $(\rho/\rho_{so})_{final}$ vs. $(\rho/\rho_{so})_{initial}$, all compositions. H - result from Horie et al. (1983).